Journal of Applied Polymer Science

# Synthesis, Characterization, and Properties of a Polyhedral Oligomeric Octadiphenylsulfonylsilsesquioxane

**Ziqian Li, Rongjie Yang**
National Engineering Research Center of Flame Retardant Materials, School of Materials, Beijing Institute of Technology, 5 South Zhongguancun Street, Haidian District, Beijing 100081, People's Republic of China
Correspondence to: R. Yang (E-mail: yrj@bit.edu.cn)

**ABSTRACT:** A novel polyhedral oligomeric octadiphenylsulfonylsilsesquioxane (ODPSS) was synthesized from octaphenylsilsesquioxane and benzenesulfonyl chloride via a Friedel–Crafts reaction with a high yield. ODPSS was identified by Fourier transform infrared spectroscopy, $^{1}$H-NMR, $^{13}$C-NMR, $^{29}$Si-NMR, matrix-assisted laser desorption/ionization time-of-flight mass spectrometry (MALDI–TOF MS), wide-angle X-ray diffraction, and elemental analysis to be a kind of polyhedral oligomeric silsesquioxane of a $T_8R_8$ structure. ODPSS exhibited superior thermal stability according to thermogravimetric analysis. Its initial thermal decomposition temperature ($T_{onset}$) was at 491°C in air and 515°C in nitrogen. Thermal and mechanical properties of epoxy resin (EP) composites with ODPSS added were studied by differential scanning calorimetry and tensile testing. The results show that the incorporation of ODPSS at a low loading content not only improved the glass-transition temperature of the EP composites but also enhanced their tensile strength. © 2014 Wiley Periodicals, Inc. J. Appl. Polym. Sci. **2014**, *131*, 40892.

**KEYWORDS:** properties and characterization; synthesis and processing; thermal properties

Received 7 February 2014; accepted 19 April 2014
**DOI: 10.1002/app.40892**

## INTRODUCTION

Hybrid materials are composites consisting of two constituents at the nanometer or molecular level. Materials mixed at the microscopic scale show characteristics between the two original components or even new properties. Polyhedral oligomeric silsesquioxanes (POSSs) as a kind of inorganic–organic hybrid material, which can be dispersed at the molecular scale or as micrometer crystalline (or amorphous) aggregates into organic polymeric matrices, have drawn much attention in recent years because of the enhancements of a variety of physical and mechanical properties in such materials.[1–10]

The general formula of POSS is $(RSiO_{3/2})_n$ (where $n$ is commonly 6, 8, or 10 and R is hydrogen or any alkyl, alkylene, aryl, arylene, or organofunctional derivatives of these groups). The field of POSS chemistry is dominated by cubelike $(RSiO_{3/2})_8$ derivatives, which are important compounds because of the rapid growth of $(RSiO_{3/2})_8$ derivative applications in recent commercial availability. Moreover, the $(RSiO_{3/2})_8$ derivatives possess designable and useful properties and can be synthesized conveniently. Interest in this area continues to increase.[11–14]

As a specific category of POSS, phenylsilsesquioxanes have high thermal stabilities and can be used in the field of flame retardants and high-temperature polymers. The most common phenylsilsesquioxane, $(PhSiO_{3/2})_8$, is very inert and insoluble and can only be functionalized via electrophilic reactions with difficulty and with poor substitutional selectivity.[15–17] However, functionalized $(PhSiO_{3/2})_8$ products are robust and highly soluble; they offer easy purification and processing. The synthesis of molecular $(RSiO_{3/2})_8$ and functionalized $(PhSiO_{3/2})_8$ via electrophilic substitution has been reviewed.[18–25]

Recently, there have been a few reports on sulfur-containing silsesquioxanes. To the best of our knowledge, most of the works reported on sulfonic acid groups containing silsesquioxanes have been used for proton-exchange membranes, dithioester-containing silsesquioxanes have been used for reversible addition–fragmentation transfer agents, and perfluoroalkylthioether-containing silsesquioxanes have been used for hydrophobic hybrid materials.[26–30] At present, there have been no studies on the synthesis of diphenylsulfone-containing POSS and the impact of sulfone on the POSS thermal stability. Sulfones are useful intermediates in a wide range of fields, including agrochemicals, pharmaceuticals, and polymers.[31–35] Diarylsulfones are widely used synthons for synthetic organic chemists, and they have many industrial applications.[36,37]

In this article, we report a new approach for synthesizing diphenylsulfone-containing POSS via a Friedel–Crafts reaction and provide the characterization results of the new POSS

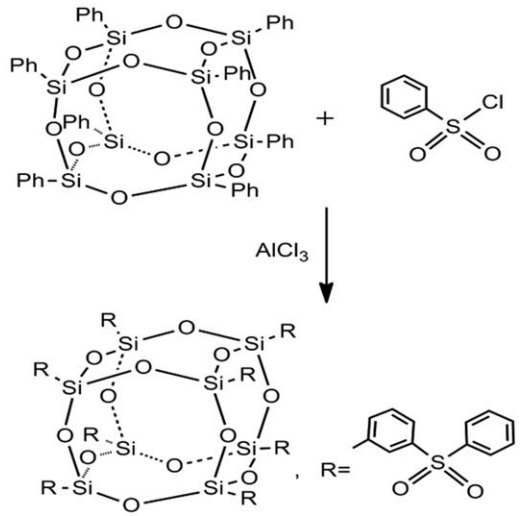


**Scheme 1.** Schematic illustration for the preparation of ODPSS.

compound. The thermal and mechanical properties of epoxy resin (EP) based on the octadiphenylsulfonylsilsesquioxane (ODPSS) were studied.

## EXPERIMENTAL

### Materials

Octaphenylsilsesquioxane [OPS; $Si_8O_{12}(C_6H_5)_8$, molecular weight ($Mw$) = 1033.2, 97%] was purchased from Hybrid Plastics. Benzenesulfonylchloride (96%) was purchased from Aladdin (China). Dichloromethane, aluminum chloride, ethanol, and *n*-hexane were purchased from Beijing Chemical Works (China). Diglycidyl ether of bisphenol A (DGEBA; E44, epoxy equivalent = 0.44 mol/100 g) was purchased from FeiChengDeYuan Chemicals Co., Ltd. 4,4′-Diaminodiphenylsulfone (DDS) was purchased from Tianjin GuangFu Fine Chemical Research Institute.

### Sulfonylation of OPS

The pathway from OPS to polyhedral oligomeric ODPSS is presented in Scheme 1. This was a Friedel–Crafts reaction. OPS (10.34 g, equivalent to 80 mmol of phenyl groups) was suspended in dichloromethane (150 mL) and benzenesulfonyl chloride (28.32 g, 160 mmol) in a 250-mL, three-necked, round-bottomed flask equipped with a magnetic stirrer and a condenser. Aluminum chloride (21.33 g, 160 mmol) was added in three parts over a 10-min period. The mixture was stirred initially at 0°C for a certain time and then allowed to warm to a temperature higher than room temperature for over 2 days. The final solution was poured into ice–water (150 g), and then, a pale yellow precipitate was collected by filtration and washed with *n*-hexane (500 mL), ethanol (1500 mL), and water (1500 mL) in turn. The resulting solid was then recovered by filtration, redissolved in 50 mL of dichloromethane, filtered through a 1-cm Celite column, reprecipitated into 700 mL of cold ethanol, and vacuum-dried for 8 h. This yielded 19.05 g (8.8 mmol, 89% yield) of pale yellow powder.

IR (KBr, $\nu$, $cm^{-1}$): 1322 (s; $SO_2$), 1304 (s; $SO_2$), 1136 (vs; $SO_2$), 1070 (vs; $SO_2$), 569 (vs; $SO_2$), 1088 (vs; Si—O—Si), 810 (s; m-CH). $^1$H-NMR (600 MHz, $CDCl_3$, $\delta$): 7.41–7.43 (t, 16H, H meta to $SO_2Ph$), 7.51–7.54 (t, 8H, meta to both POSS and $SO_2Ph$), 7.66–7.68 (t, 8H, para to $SO_2Ph$), 7.83–7.84 (d, 16H, ortho to $SO_2Ph$), 8.04–8.05 (d, 8H, ortho to $SO_2Ph$ and para to POSS), 8.08–8.09 (d, 8H, ortho to POSS and para to $SO_2Ph$), 8.35 (s, 8H, ortho to both POSS and $SO_2Ph$). $^{13}$C-NMR (151 MHz, $CDCl_3$, $\delta$): 141.8 (C—$SO_2Ph$), 141.0 (C—$SO_2Ph$), 138.8, 133.4, 132.9, 130.7, 130.2, 129.7, 129.4, 127.6. $^{29}$Si-NMR (119 MHz, $CDCl_3$, $\delta$): −79.34 (Si—$PhSO_2Ph$). Matrix-assisted laser desorption/ionization time-of-flight mass spectrometry [MALDI–TOF MS; mass-to-charge ratio ($m/z$; %)]: $[M + Na]^+$ calculated for ODPSS = 2177.7 and found = 2175.8 (100). Anal. Calcd for ODPSS: C, 53.51%; H, 3.37%; S, 11.90%. Found: C, 52.58%; H, 3.29%; S, 11.74%.

### Preparation of the Cured EPs

The cured EPs were obtained with a thermal curing process. At first, the ODPSS was dispersed in DGEBA by mechanical stirring at 140°C for 1 h, and it dissolved in DGEBA. The mixture was a homogeneous and transparent liquid. After that, the curing agent DDS was added to the amount of DGEBA. To study the effect of ODPSS in EP, two EPs of different curing degrees, which were abbreviated as EP1 and EP2, were chosen. The equivalent weight ratio of DGEBA to DDS was 4.5:1 for the cured EP1, and it was 3.7:1 for EP2. The EPs were cured at 180°C for 4 h. The contents of the ODPSS in the EP composites are listed in Tables III and IV (shown later).

### Instrumentation

The FTIR spectra were record on a Nicolet 6700 IR spectrometer. The spectra were collected at 32 scans with a spectral resolution of 4 $cm^{-1}$.

$^1$H-NMR, $^{13}$C-NMR, and $^{29}$Si-NMR spectra were recorded on Bruker Avance 600 NMR spectrometer operating in Fourier transform mode. $CDCl_3$ was used as the solvent, and the solution was measured with tetramethylsilane as an internal reference. $^1$H-NMR spectra were collected at 600.2 MHz with a 1233.5-Hz spectral width. $^{13}$C-NMR spectra were collected at 150.9 MHz with a 36,057.7-Hz spectral width. $^{29}$Si-NMR spectra were collected at 119.2 MHz with a 9566.3-Hz spectra width.

MALDI–TOF MS was performed with a Bruker BIFLEX III device. It was equipped with a pulsed nitrogen laser ($\lambda$ = 337 nm, pulse width = 3 ns, and average power = 5 mW at 20 Hz). The extraction voltage in the TOF analyzers was 20 kV, and ions were obtained by irradiation just above the threshold laser power (ca. one-third of the average laser power). The samples were measured in the positive-ion mode. Usually, 50 spectra were accumulated. The *a*-cyano-4-hydroxycinnamic acid as the matrix substance was used for MALDI–TOF MS, and the salts were a mixture of NaCl and KCl.

Elemental analysis of C, H, and S were carried out with a Vario EL Cube CHNOS elemental analyzer (Germany). The $O_2$ gas was used as fuel, and helium gas was used as a carrier gas and to provide an inert atmosphere. The operating temperatures of the combustion tube and reduction tube were 1150 and 850°C, respectively.

The wide-angle X-ray diffraction (WAXD) analysis was achieved with an X'Pert PRP diffractometer system; a step scan with a

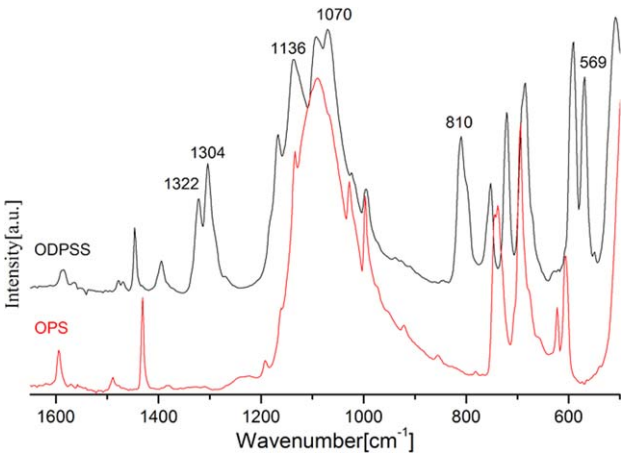


**Figure 1.** FTIR spectra of the OPS and ODPSS. [Color figure can be viewed in the online issue, which is available at wileyonlinelibrary.com.]

step size of 0.0330° and a scan step time of 19.6850 s. Cu K$\alpha$ radiation was used with a copper target over the $2\theta$ range 5–70°.

Density was measured with an automatic density analyzer (ULTRAPYC 1200e).

Thermogravimetric analysis (TGA) was performed with a Netzsch 209 F1 thermal analyzer at a heating rate of 10°C/min under nitrogen and air atmospheres, and the temperature ranged from 45 to 850°C.

Differential scanning calorimetry (DSC) measurements were performed on a Netzsch DSC 204 F1 instrument (Germany). The DSC instrument was set for the temperature range 30–400°C. Samples (5–10 mg) were tested at a heating rate of 10°C/min under a nitrogen flow of 20 $cm^3$/min. The obtained data was extracted from second heating.

Tensile dog-bone-shaped samples (4-mm neck thickness × 10-mm neck width × 80-mm neck length) produced according to GB/T 1040–2006 were obtained after casting. The tensile tests were carried out on a DXLL-5000 electronic universal mechanical testing machine controlled by an extensometer at an extension rate of 50 mm/min. The reported data was the average of the results extracted from a minimum of five specimens. The measurements were carried out at room temperature and at a relative humidity of 65%.

## RESULTS AND DISCUSSION

### Characterization of ODPSS

Polyhedral oligomeric octadiphenylsulfonyl silsesquioxane (ODPSS) was successfully synthesized by the one-step aromatic electrophilic sulfonylation of OPS with an excess of benzenesulfonyl chloride (Scheme 1). ODPSS was characterized by FTIR spectroscopy, $^1$H-NMR, $^{13}$C-NMR, $^{29}$Si-NMR, MALDI–TOF MS, WAXD, and element analysis. ODPSS in pale yellow powder had a true density of 1.427 g/$cm^3$.

The sulfonylation of OPS was confirmed by FTIR spectroscopy, NMR spectroscopy, MALDI–TOF mass spectrometry, and elemental analysis. The FTIR spectra of the POSS powders before and after the sulfonylation reaction are shown in Figure 1. The broad band at 1088 $cm^{-1}$ corresponded to the asymmetric stretching of the Si—O—Si groups of POSS. The FTIR spectrum of ODPSS (Figure 1) showed a strong peak at 569 $cm^{-1}$, which resulted from the $SO_2$ group; peaks at 1070 and 1136 $cm^{-1}$ due to the $SO_2$ symmetric stretching vibrations; 1304 and 1322 $cm^{-1}$ due to the $SO_2$ asymmetric stretching vibrations; and 810 $cm^{-1}$ due to the metasubstituted aromatic ring. These FTIR spectra indicated characteristics of the ODPSS compound.

$^1$H-NMR spectroscopy (Figure 2) showed seven peaks in the aromatic region due to diphenylsulfone groups. Four nonequivalent protons due to a metadisubstituted phenyl group carrying $Si_8O_{12}$ and $SO_2Ph$ groups and three nonequivalent protons due to a monosubstituted phenyl group were observed. Ten peaks were observed in the aromatic region of the $^{13}$C-NMR spectrum (Figure 3). The starting OPS reagent was a monosubstituted phenyl compound with four nonequivalent ArCH carbon environments. $^{13}$C-NMR of ODPSS showed peaks at 141.0 and 141.8 ppm due to the carbon attached to the sulfone, with an upper field shift on the carbon atoms of the sulfonylated phenyl rings. The $^1$H-NMR and $^{13}$C-NMR spectra suggested metasubstitution had occurred as expected.

The sensitivity of the $^{29}$Si chemical shifts to changes in the substituents in the POSS cage caused us to use $^{29}$Si-NMR spectroscopy to determine the degree of substitution in the reaction. The $^{29}$Si-NMR spectra of the compounds confirmed their complete conversion from the parent OPS. The $^{29}$Si-NMR spectrum of ODPSS (Figure 4) showed a singlet at −79.34 ppm; this was attributed to silicon attached to the diphenylsulfone group. Only one peak observed in the $^{29}$Si-NMR spectrum implied that all of the Si atoms of the ODPSS were in the same environment.

The NMR spectra of the ODPSS supported by MALDI–TOF mass analysis is shown in Figure 5. The theoretical *m*/*z* values for the eight degrees of substitution of ODPSS should have

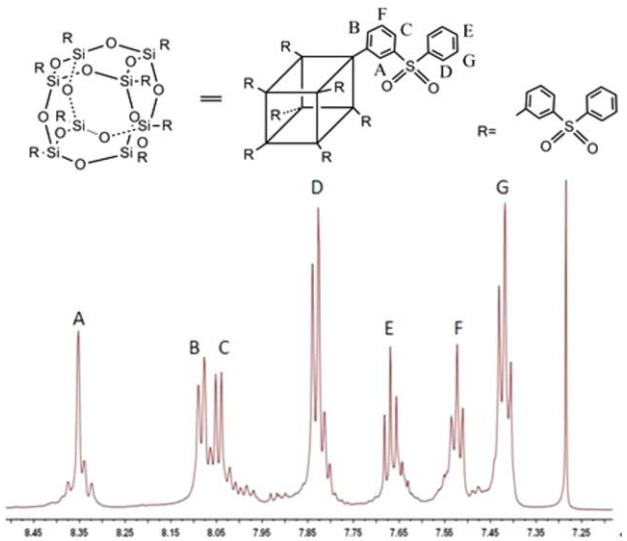


**Figure 2.** $^1$H-NMR spectrum of ODPSS in $CDCl_3$. [Color figure can be viewed in the online issue, which is available at wileyonlinelibrary.com.]

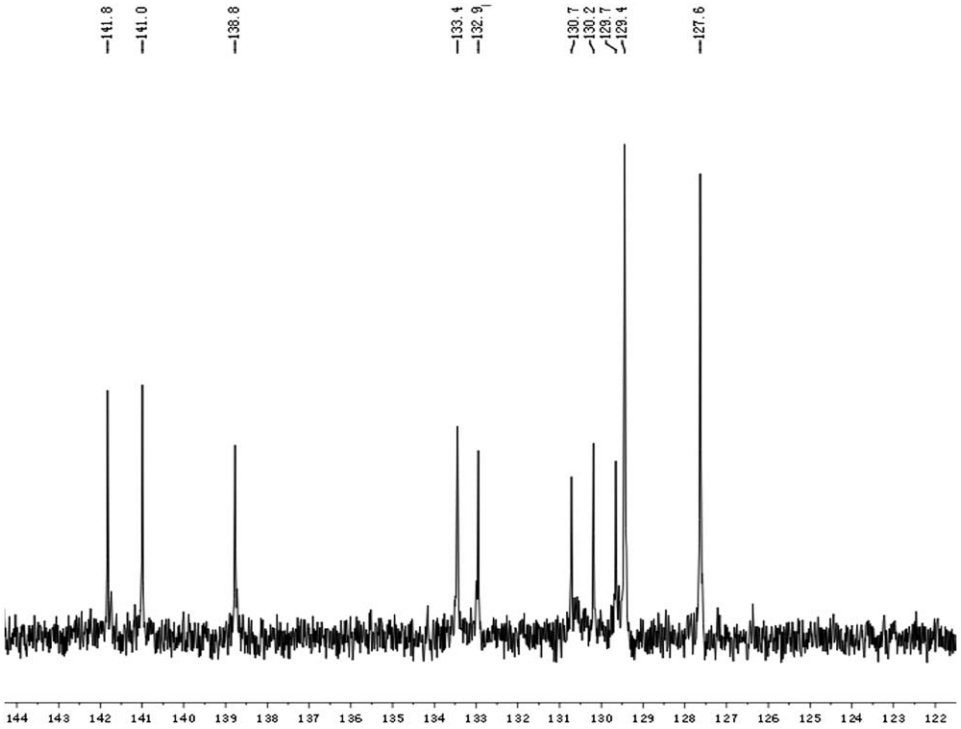


**Figure 3.** $^{13}$C-NMR spectrum of ODPSS in $CDCl_3$.

been 2154.7 ($m/z$). The detected molecular ions corresponding to the ionization with $Na^+$ were 2175.8 $[+Na]^+$ ($m/z$). We verified that the degrees of substitution of the sulfonylation products were eight.

The elemental analysis data of carbon, hydrogen, and sulfur of ODPSS were also close to the theoretical values.

**Crystalline ODPSS**

It was of interest to examine the behavior of crystallization of the ODPSS because it contained an inorganic silica-like core decorated with huge octadiphenylsulfonyl groups. Shown in Figure 6 is the pattern of WAXD of ODPSS. The appearance of sharp diffraction peaks indicates that ODPSS was a crystalline material. The WAXD pattern of ODPSS had two dominant

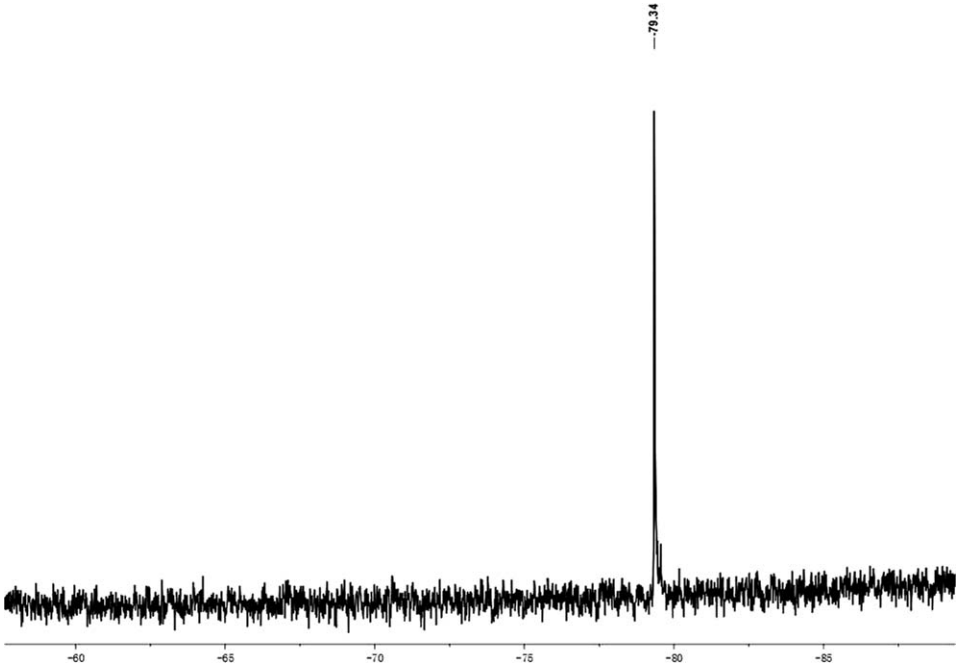


**Figure 4.** $^{29}$Si-NMR spectrum of ODPSS in $CDCl_3$.

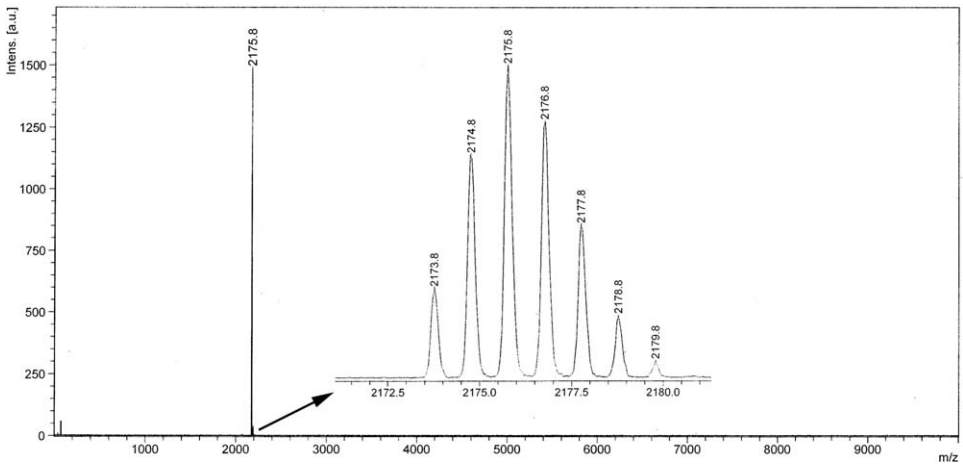


**Figure 5.** MALDI–TOF mass spectrum of ODPSS.

characteristic peaks at about $2\theta$ values of 6.1 and 6.4°. These peaks represented the periodic distances of 1.45 and 1.38 nm and were assigned to the (100) and (001) planes, respectively. The 1.45-nm distance likely corresponded to the overall dimensions of the ODPSS molecule.[38]

### Thermal Properties of ODPSS

The TGA and derivative thermogravimetry (DTG) curves of OPS and ODPSS in a nitrogen atmosphere are presented in Figure 7. Table I lists the TGA and DTG results for OPS and ODPSS in nitrogen. We observed the thermal decomposition data, and the initial thermal decomposition temperature ($T_{onset}$) of OPS (466°C) was about 49°C lower than the $T_{onset}$ of ODPSS (515°C), and the temperature at maximum mass loss rate ($T_{max}$) of OPS possessed two values (456 and 611°C) and that of ODPSS possessed one (549°C). $T_{onset}$ is defined as the temperature at which 5% mass loss occurs, and $T_{max}$ is defined as the temperature at maximum mass loss rate. These indicated that ODPSS was more thermally stable than OPS. The mass losses of OPS and ODPSS in the temperature range 45–400°C were similar; then, both of them degraded rapidly with increasing temperature. This corresponded to the degradation of the organic groups in the silsesquioxanes. The residue of ODPSS at 800°C was 53%; this was 21% lower than the residue of OPS in nitrogen.

The TGA and DTG curves of OPS and ODPSS in an air atmosphere are presented in Figure 8. Table II lists the TGA and DTG results for OPS and ODPSS in air. Both OPS and ODPSS went through two rapid degradation stages. The first degradation stage of ODPSS appeared later than that of OPS. The $T_{onset}$ of OPS (447°C) was about 44°C lower than the $T_{onset}$ of ODPSS (491°C). The residue of ODPSS at 800°C was 23%; this was 14% lower than the residue of OPS in air.

In addition, OPS and ODPSS in air are not as stable as in nitrogen because the presence of oxygen may have promoted the thermal oxidative degradation of the organic fraction in silsesquioxanes. The almost white residue of ODPSS after treatment was 23% of the initial weight and could be accounted for by the quantitative oxidative transformation of ODPSS to silica. The ceramic yield for OPS was 37%; this was close to the calculated values for pure silica (40%).[39]

The DSC curve for ODPSS at a heating rate of 10°C/min in $N_2$ is shown in Figure 9. In the 30–400°C range, we observed a

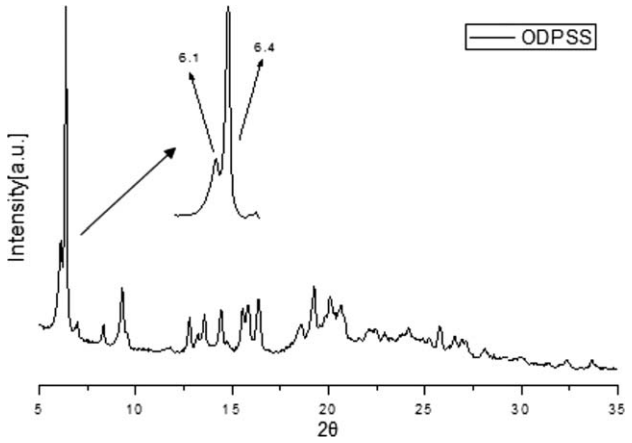


**Figure 6.** WAXD pattern of ODPSS.

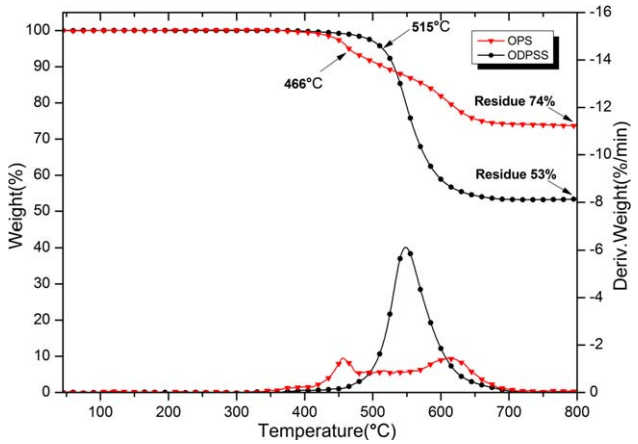


**Figure 7.** TGA and DTG curves of OPS and ODPSS in nitrogen. [Color figure can be viewed in the online issue, which is available at wileyonlinelibrary.com.]

**Table I.** TGA and DTG Results for OPS and ODPSS in Nitrogen

| Assignment | $T_{onset}$ (°C) | $T_{max}$ (°C) | Residual yield at 800°C (%) |
|---|---|---|---|
| OPS | 466 | 456 and 611 | 74 |
| ODPSS | 515 | 549 | 53 |

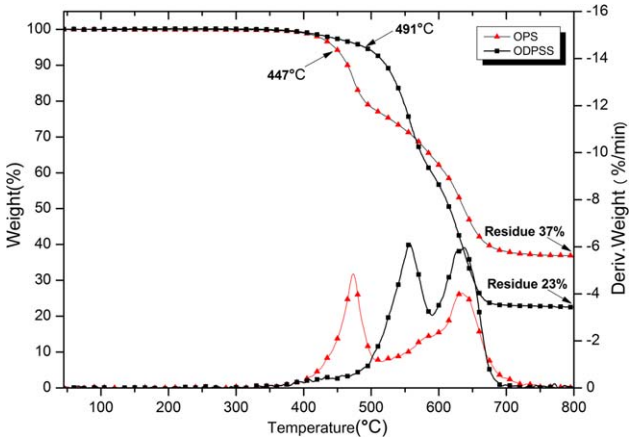


**Figure 8.** TGA and DTG curves of OPS and ODPSS in air. [Color figure can be viewed in the online issue, which is available at wileyonlinelibrary.com.]

glass-transition temperature ($T_g$) of ODPSS. The presence of $T_g$ of ODPSS may have been due to the fact that the conformation of huge diphenylsulfone groups changed under heating. These movements of huge functional groups induced the irregular arrangement of organic groups in the ODPSS.

### Tensile Strength of the Cured EP Composites

The average data of the tensile strength of the cured EP1 and EP2 composites are given in Tables III and IV. Figures 10 and 11 show the tensile strengths of the cured EP1 and EP2 composites with standard deviations, respectively. As the amount of ODPSS increased, the ODPSS/EP composites exhibited a higher tensile strength than the EP control. The tensile strength of EP1–2% was 61 MPa; this increased about 35% compared with that of the EP1 control. The tensile strength of EP2–4% was 67 MPa; this increased about 31% compared with that of the EP2 control.

The introduction of ODPSS imparted a good reinforcement effect to the composites because the ODPSS with rigid structures could not undergo large tensile deformation under the stretching force; this efficiently retarded the crack growth.[40] The compatibility between ODPSS and EP had a good effect on the tensile properties of the materials. On the other hand, the initial improvement could also be ascribed to the presence of a small fraction of very well dispersed ODPSS. However, with the increase in the loading content, ODPSS aggregated and formed larger POSS crystal agglomerates. The presence of those large agglomerates having low adhesion with the matrix weakened the composite. The interface area between the EP matrix and the nanofiller was also dramatically reduced; thus, the agglomerates of ODPSS caused the low tensile strength of the EP composites.[41]

**Table II.** TGA and DTG Results for OPS and ODPSS in Air

| Assignment | $T_{onset}$ (°C) | $T_{max}$ (°C) | Residual yield at 800°C (%) |
|---|---|---|---|
| OPS | 447 | 474 and 633 | 37 |
| ODPSS | 491 | 557 and 638 | 23 |

**Table III.** Compositions and Properties of the EP1 Systems

| Samples ID | Cured EP (wt %) | Content of ODPSS (wt %) | Tensile strength (MPa) | $T_g$ (°C) |
|---|---|---|---|---|
| EP1-control | 100 | 0 | 45 | 122 |
| EP1-1% | 99 | 1 | 50 | 136 |
| EP1-2% | 98 | 2 | 61 | 139 |
| EP1-3% | 97 | 3 | 51 | 143 |
| EP1-4% | 96 | 4 | 49 | 144 |
| EP1-5% | 95 | 5 | 49 | 138 |

**Table IV.** Compositions and Properties of the EP2 Systems

| Sample ID | Cured EP (wt %) | Content of ODPSS (wt %) | Tensile strength (MPa) | $T_g$ (°C) |
|---|---|---|---|---|
| EP2-control | 100 | 0 | 51 | 178 |
| EP2-1% | 99 | 1 | 58 | 180 |
| EP2-2% | 98 | 2 | 60 | 185 |
| EP2-3% | 97 | 3 | 63 | 187 |
| EP2-4% | 96 | 4 | 67 | 188 |
| EP2-5% | 95 | 5 | 59 | 182 |
| EP2-6% | 94 | 6 | 58 | 182 |

### Thermal Properties of the EP Composites

The $T_g$ values of the EP composites were measured by DSC. The DSC curves of the samples of EP1 and EP2 are displayed in Figures 12 and 13, and the results are summarized in Tables III and IV, respectively. As the amount of ODPSS increased, the

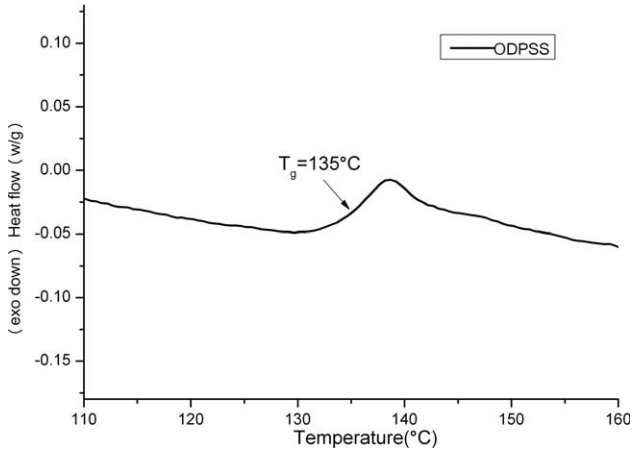


**Figure 9.** DSC curve of ODPSS.

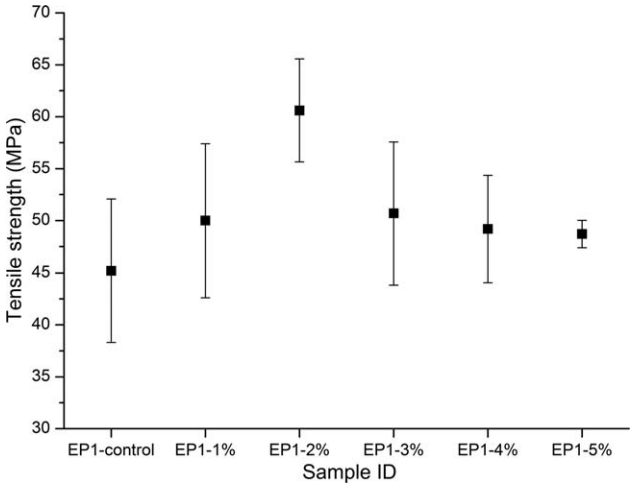


**Figure 10.** Tensile strength of the cured EP1 composites.

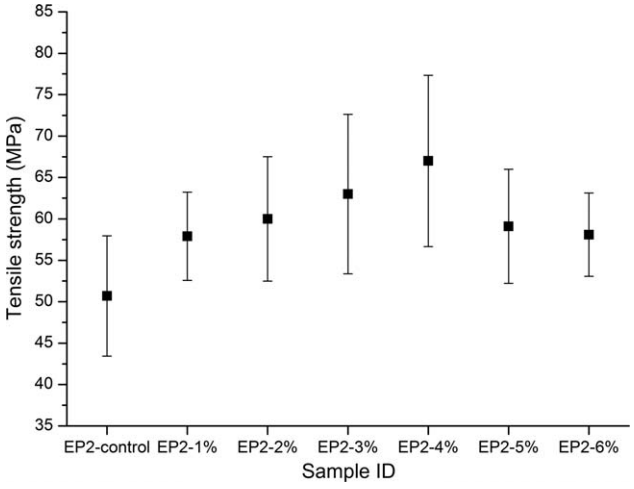


**Figure 11.** Tensile strength of the cured EP2 composites.

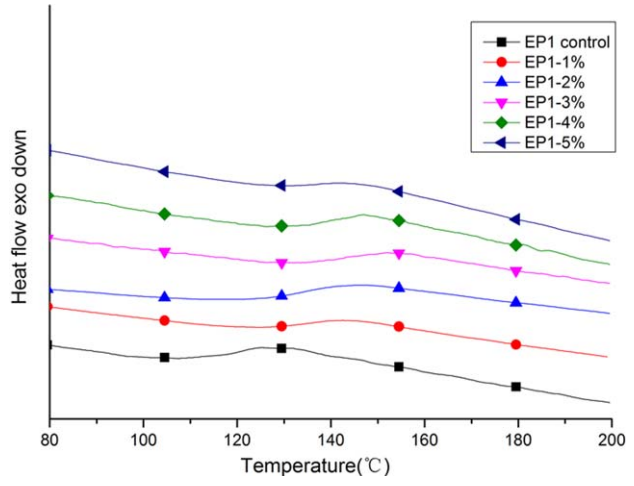


**Figure 12.** DSC curves of the EP1 composites. [Color figure can be viewed in the online issue, which is available at wileyonlinelibrary.com.]

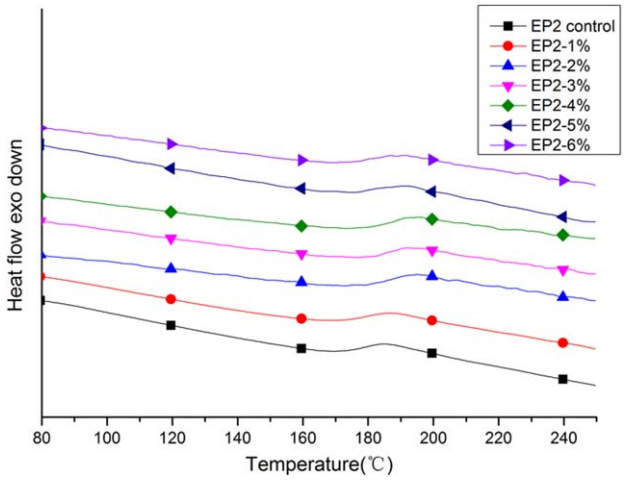


**Figure 13.** DSC curves of the EP2 composites. [Color figure can be viewed in the online issue, which is available at wileyonlinelibrary.com.]

ODPSS/EP composites with less than 5 wt % ODPSS compositions exhibited a higher $T_g$ than the EP control. The $T_g$ of EP1–4% (144°C) was about 22°C higher than the $T_g$ of the EP1 control (122°C). The $T_g$ of EP2–4% (188°C) was about 10°C higher than the $T_g$ of EP2 control (178°C). These were attributed to the rigid structures of ODPSS introduced to the composites; these acted as anchor points. In addition, ODPSS owned a similar molecular structure to DDS, and this indicated good compatibility between ODPSS and DGEBA/DDS. This may have been the reason for the unique $T_g$ of each ODPSS/EP composite.

Such an increase in $T_g$, however, was not fully monotonic. With increasing content of ODPSS, the $T_g$ of the resins first increased and then decreased. As the crosslinking density increased with the DDS concentration, the $T_g$ of the EP2 control was much higher than that of EP1 control. In other words, the $T_g$ of the EP was greatly affected by the curing degree.[42] Therefore, $T_g$ of EP was increased when ODPSS was added at low levels because rigid molecules were introduced to hinder the movement of the molecular chain. Nevertheless, $T_g$ of EP decreased when ODPSS was added at high levels because ODPSS restricted the crosslinking density.

## CONCLUSIONS

A novel organic–inorganic hybrid polyhedral oligomeric ODPSS $[(SiO_{3/2})_8(C_6H_4SO_2C_6H_5)_8]$ was successfully synthesized through the sulfonylation of OPS. The chemical structure of ODPSS was characterized by FTIR spectroscopy, $^{1}$H-NMR, $^{13}$C-NMR, $^{29}$Si-NMR, MALDI–TOF MS, WAXD, and elemental analyses. FTIR spectroscopy revealed the sulfonylation of OPS. NMR and MALDI–TOF MS suggested that ODPSS had eight metasubstitution octadiphenylsulfonyl groups. WAXD indicated that the ODPSS was crystalline. DSC and TGA uncovered the high thermal stability of ODPSS in both nitrogen and air. The incorporation of ODPSS into EP at a low loading content improved the $T_g$ and tensile strength of the EP composites. As POSS could evolve into a ceramic superficial layer during the earlier stage of combustion, an interesting application of POSS could be in the fire retardancy of polymeric materials.[43–49]

ODPSS is expected to have important applications in high-temperature-resistant and flame-retardant polymer materials.

## REFERENCES


1. Escudé, N. C.; Chen, E. Y. X. *Chem. Mater.* **2009**, *21*, 5743.
2. Wu, S.; Hayakawa, T.; Kikuchi, R.; Grunzinger, S. J.; Kakimoto, M.-A.; Oikawa, H. *Macromolecules* **2007**, *40*, 5698.
3. Liang, K.; Li, G.; Toghiani, H.; Koo, J. H.; Pittman, C. U. *Chem. Mater.* **2006**, *18*, 301.
4. Mather, P. T.; Jeon, H. G.; Romo-Uribe, A.; Haddad, T. S.; Lichtenhan, J. D. *Macromolecules* **1999**, *32*, 1194.
5. Huang, J.-C.; He, C.-B.; Xiao, Y.; Mya, K. Y.; Dai, J.; Siow, Y. P. *Polymer* **2003**, *44*, 4491.
6. Phillips, S. H.; Haddad, T. S.; Tomczak, S. *J. Curr. Opin. Solid State Mater. Sci.* **2004**, *8*, 21.
7. Iyer, P.; Coleman, M. R. *J. Appl. Polym. Sci.* **2008**, *108*, 2691.
8. Zhao, Y.; Schiraldi, D. A. *Polymer* **2005**, *46*, 11640.
9. Wu, J.; Mather, P. T. *Polym. Rev.* **2009**, *49*, 25.
10. Liu, Y.; Zheng, S.; Nie, K. *Polymer* **2005**, *46*, 12016.
11. Lickiss, P. D.; Rataboul, F. *Adv. Organomet. Chem.* **2008**, *57*, 1.
12. Li, G.; Wang, L.; Ni, H.; Pittman, C. U., Jr. *J. Inorg. Organomet. Polym.* **2001**, *11*, 123.
13. Ayandele, E.; Sarkar, B.; Alexandridis, P. *Nanomaterials* **2012**, *2*, 445.
14. Laine, R.; Tamaki, R.; Choi, J. W.O. Pat. WO/2002/100867 (2002).
15. Roll, M. F.; Asuncion, M. Z.; Kampf, J.; Laine, R. M. *ACS Nano* **2008**, *2*, 320.
16. Brick, C.; Tamaki, R.; Kim, S.-G.; Asuncion, M.; Roll, M.; Nemoto, T.; Ouchi, Y.; Chujo, Y.; Laine, R. *Macromolecules* **2005**, *38*, 4655.
17. Fan, H.; He, J.; Yang, R. *J. Appl. Polym. Sci.* **2013**, *127*, 463.
18. David, B.; Cordes, P. D. L.; Rataboul, F. *Chem. Rev.* **2010**, *110*, 2081.
19. Laine, R. M.; Roll, M. F. *Macromolecules* **2011**, *44*, 1073.
20. Lichtenhan, J. D. *Comments Inorg. Chem.* **1995**, *17*, 115.
21. Kuo, S.-W.; Chang, F.-C. *Prog. Polym. Sci.* **2011**, *36*, 1649.
22. Hartmann-Thompson, C.; Nowak, R. M.; Bruza, K. J.; Thomas, L. S.; Meier, D. J. W.O. Pat. WO/2008/127645 (2008).
23. Brick, C. M.; Chan, E. R.; Glotzer, S. C.; Marchal, J. C.; Martin, D. C.; Laine, R. M. *Adv. Mater.* **2007**, *19*, 82.
24. Liu, Y.; Shi, Z.; Xu, H.; Fang, J.; Ma, X.; Yin, J. *Macromolecules* **2010**, *43*, 6731.
25. Sulaiman, S. Ph.D. Thesis, University of Michigan, **2011**.
26. Hartmann-Thompson, C.; Merrington, A.; Carver, P. I.; Keeley, D. L.; Rousseau, J. L.; Hucul, D.; Bruza, K. J.; Thomas, L. S.; Keinath, S. E.; Nowak, R. M.; Katona, D. M.; Santurri, P. R. *J. Appl. Polym. Sci.* **2008**, *110*, 958.
27. Subianto, S.; Mistry, M. K.; Choudhury, N. R.; Dutta, N. K.; Knott, R. *ACS Appl. Mater. Interfaces* **2009**, *1*, 1173.
28. Zhang, W.; Liu, L.; Zhuang, X.; Li, X.; Bai, J.; Chen, Y. *J. Polym. Sci. Part A: Polym. Chem.* **2008**, *46*, 7049.
29. Zhang, W.; Fang, B.; Walther, A.; Müller, A. H. *Macromolecules* **2009**, *42*, 2563.
30. Xu, J.; Li, X.; Cho, C. M.; Toh, C. L.; Shen, L.; Mya, K. Y.; Lu, X.; He, C. *J. Mater. Chem.* **2009**, *19*, 4740.
31. Weijlard, J.; Messerly, J. P. U.S. Pat. 2,385,899 (1945).
32. Michaely, W.; Krattz, G. W. U.S. Pat. 4,780,127 (1988).
33. MacKinnon, S. M.; Wang, Z. Y. *Macromolecules* **1998**, *31*, 7970.
34. Finocchiaro, P.; Montaudo, G.; Mertoli, P.; Puglisi, C.; Samperi, F. *Macromol. Chem. Phys.* **1996**, *197*, 1007.
35. Robsein, R. L.; Straw, J. J.; Fahey, D. R. U.S. Pat. 5,260,489 (1993).
36. Magnus, P. D. *Tetrahedron* **1977**, *33*, 2019.
37. Field, L. *Synthesis* **1978**, *10*, 713.
38. Takamura, N.; Viculis, L.; Zhang, C.; Laine, R. M. *Polym. Int.* **2007**, *56*, 1378.
39. Fina, A.; Tabuani, D.; Carniato, F.; Frache, A.; Boccaleri, E.; Camino, G. *Thermochim. Acta* **2006**, *440*, 36.
40. Ruiz-Pérez, L.; Royston, G. J.; Fairclough, J. P. A.; Ryan, A. *J. Polymer* **2008**, *49*, 4475.
41. Sánchez-Soto, M.; Schiraldi, D. A.; Illescas, S. *Eur. Polym. J.* **2009**, *45*, 341.
42. Wei, J.; Hawley, M. C.; Delong, J. D. *Polym. Eng. Sci.* **1993**, *33*, 1132.
43. Zanetti, M.; Kashiwagi, T.; Falqui, L.; Camino, G. *Chem. Mat.* **2002**, *14*, 881.
44. Zhang, W.; Li, X.; Fan, H.; Yang, R. *Polym. Degrad. Stab.* **2012**, *97*, 2241.
45. Zhang, W.; Li, X.; Li, L.; Yang, R. *Polym. Degrad. Stab.* **2012**, *97*, 1041.
46. Zhang, W.; Li, X.; Yang, R. *Polym. Degrad. Stab.* **2011**, *96*, 2167.
47. Zhang, W.; Li, X.; Yang, R. *Polym. Degrad. Stab.* **2011**, *96*, 1821.
48. Zhang, W.; Li, X.; Yang, R. *Polym. Degrad. Stab.* **2012**, *97*, 1314.
49. Li, L.; Li, X.; Yang, R. *J. Appl. Polym. Sci.* **2012**, *124*, 3807.